https://doi.org/10.5194/egusphere-2025-874
Preprint. Discussion started: 2 June 2025

Identifying MBL cloud boundaries and phase over the Southern Ocean using airborne radar and in-situ measurements during the SOCRATES campaign

Anik Das[1], Baike Xi[1], Xiaojian Zheng[1,a], and Xiquan Dong[1]*

[1]Department of Hydrology and Atmospheric Sciences, University of Arizona, Tucson, AZ, USA
[a]Now at Environmental Science Division, Argonne National Laboratory, Lemont, IL, USA

Correspondence: Xiquan Dong (xdong@arizona.edu)

Abstract.

The Southern Ocean Clouds, Radiation, Aerosol Transport Experimental Study (SOCRATES) was an aircraft-based campaign (Jan 15 – Feb 26, 2018) using in-situ probes and remote sensors, targeting low-level clouds over the Southern Ocean (SO). A novel methodology was developed to identify cloud boundaries and classify cloud phases in marine boundary layer (MBL) clouds using airborne HIAPER Cloud Radar (HCR) and in-situ CDP+2D-S measurements. Cloud boundaries were determined using HCR reflectivity and spectrum width gradients. Single-layer low-level clouds accounted for ~85% of observed cases. HCR-derived boundaries showed decent agreement with the Ceilometer and Micropulse lidar (MPL)-measurements during the Measurement of Aerosols, Radiation, and Clouds (MARCUS) ship-based campaign, with mean base and top differences of 0.04 km and 0.29 km. Additionally, HCR-derived cloud base heights correlated well (R = 0.78) with HSRL observations. A reflectivity–liquid water content (Z-LWC) relationship, $LWC = 0.70Z^{0.29}$, was derived to retrieve LWC and liquid water path (LWP) from HCR profiles. The estimated LWP closely matched MARCUS microwave radiometer (MWR) retrievals, with a mean difference of 9.24 g/m². Cloud phase was classified using HCR-measurements, temperature, and LWP. Among single-layered LOW clouds, 48.8% were classified as liquid, 23.3% mixed-phase, and 6.9% ice, with additional categories identified: drizzle (16.2%), rain (3.4%), and snow (1.5%). The classification algorithm demonstrated over 90% agreement with established phase detection methods. This study provides a robust framework for boundary and phase detection of MBL clouds, offering valuable insights into cloud microphysical processes over the SO and supporting future efforts in satellite algorithm development and climate model evaluation.

1. Introduction

The Southern Ocean (SO) clouds contain mainly low-level clouds, which significantly influence the regional radiation budget (60°S latitude, encircling Antarctica). Yet global climate models struggle to simulate them accurately (Bodas-Salcedo et al., 2016; Kay et al., 2016; Trenberth & Fasullo, 2010; Wang et al., 2018, McCoy et al., 2014; D'Alessandro et al., 2021). Low-level marine boundary layer (MBL) clouds over the SO exhibit a high prevalence of SLW, with ~80% containing SLW across a temperature range of -40 to 0°C (Hu et al., 2010). Their macrophysical and microphysical properties differ significantly from subtropical MBL clouds, with dominant warm liquid clouds (Dong et al., 2014; Wu et al, 2020; Zhao et al., 2020), and from Arctic mixed-phase clouds, which feature liquid tops and ice-dominated bases (Qiu et al., 2015; Jackson et al., 2012; Moser et al., 2023). Understanding the dominant cloud phase and spatial homogeneity of low-level SO clouds is critical for improving cloud

https://doi.org/10.5194/egusphere-2025-874
Preprint. Discussion started: 2 June 2025

parameterizations and refining global climate model predictions (Zhao et al., 2023; Liu et al., 2023).

Identifying cloud phase is crucial for accurately retrieving cloud macrophysical and microphysical properties, as most retrieval algorithms are phase- and region-specific (Shupe, 2007). Various methods have been developed for classifying cloud type, phase, and hydrometeors over the SO (e.g., Xi et al., 2022; Desai et al., 2023; Schima et al., 2022; D'Alessandro et al., 2021, 2019; Romatschke & Vivekanandan, 2022; Atlas et al., 2021; Zaremba et al., 2020) and Arctic clouds (e.g., Shupe, 2007; Korelov & Milbrandt, 2022; Mioche et al., 2015; Matus & L'Ecuyer, 2017), each with varying performance based on retrieval methods and assumptions. Compared to ground-based measurements, aircraft in-situ observations provide more reliable datasets, minimizing retrieval uncertainties by directly sampling cloud boundaries and interiors. Additionally, onboard radar and lidar experience less attenuation than ground-based sensors (Ewald et al., 2021). Cloud phase retrieval remains highly dependent on observational scale, sample size, and viewing direction. Ground-based radar and lidar more accurately capture low-level clouds but suffer attenuation when observing higher altitudes. On the other hand, satellite-based sensors effectively detect high-level clouds but may struggle with low-level cloud retrieval due to signal attenuation (Dong et al., 2025).

The Southern Ocean Clouds, Radiation, Aerosol Transport Experimental Study (SOCRATES) provided a valuable dataset for investigating marine boundary layer (MBL) clouds over the SO. The airborne in-situ probes— Cloud Droplet Probe (CDP) and Two-Dimensional, Stereo, Particle Imaging Probe (2D-S), and remote sensors— the 94.4 GHz (W-band) HIAPER Cloud Radar (GV-HCR) and the 532 nm High Spectra Resolution Lidar (NCAR-HSRL) onboard the research aircrafts during SOCRATES enabled direct observations of precipitation, cloud particles, and aerosols across different cloud layers, providing vertical profiles to characterize MBL structure and the free troposphere. Previous studies utilizing SOCRATES measurements for cloud phase classification include a multinomial logistic regression (MLR) method by D'Alessandro (2021) which used in-situ cloud and drizzle probe (CDP & 2D-S) measurements to estimate cloud phase heterogeneity and frequency distributions. This method identified significant SLW and ice-phase clouds and was later refined by Schima (2022) to address inconsistencies. Romatschke & Vivekanandan (2022) presented a fuzzy logic scheme that classifies cloud hydrometeor types as a time-height profile using cloud radar-lidar data. Atlas (2021) developed the University of Washington Ice-Liquid Discriminator (UWILD), a random forest-based single-particle phase classification method for binary 2D-S images.

Remote sensing offers 2-dimensional cloud profiles, complementing the size-resolved distributions captured by in-situ measurements. However, relying solely on either method can introduce discrepancies—in-situ probes detect particles only at the aircraft's altitude, while radar-lidar profiles provide vertical cloud structure but suffers near-surface contamination due to surface clutter (Dong et al., 2025). Therefore, integrating in-situ sampling with remote sensing provides significant advantages for studying atmospheric processes (Wang et al., 2012). Lidar, with its shorter wavelength, resolves aerosols, ice precipitation, optically thin clouds, and cloud boundaries (Wang et al., 2012, 2009; McGill et al., 2002), but is easily attenuated by thicker cloud layers, such as liquid clouds (Sassen, 1991). Therefore, this study focuses on developing a method solely based on radar measurements to identify cloud boundaries and phase in MBL clouds.

In this study, we aim to use a combination of both in-situ and radar-based measurements during SOCRATES to:

1. Develop a method to identify cloud base and top heights using airborne HCR radar reflectivity and spectrum width gradient, offering cloud boundary estimation without radiosonde or drop-sonde data. Further, derive an LWC-Z exponential relationship

https://doi.org/10.5194/egusphere-2025-874
Preprint. Discussion started: 2 June 2025

from in-situ measured liquid water content (LWC) and calculated reflectivity (Z) from CDP and 2D-S probes and apply it to HCR reflectivity profiles to obtain radar-based LWC and liquid water path (LWP).

2. Develop a cloud phase estimation method for classified low-level clouds sampled during SOCRATES, using a combination of HCR measurements, temperature profiles and estimated LWPs. Compare the classified phase categories with existing products over the SO.

The manuscript is organized in the following manner: Section 2 contains a brief introduction to the SOCRATES campaign, descriptions of the remote sensors and in-situ probes, along with a LWC-Z relationship derived using in-situ measured LWC and calculated reflectivity (Z) from in-situ measurements. The classification methodology for low-level clouds based on cloud-base and -top heights is described in Section 3. Section 4 contains the cloud phase classification methodology along with an extensive evaluation through comparisons with existing phase-determination methods and results from other campaigns over the SO. Finally, summary and conclusions are presented in Section 5.

2 SOCRATES observations and deriving LWC-Z relationship

2.1 SOCRATES in-situ and remote sensing datasets

A brief overview of the SOCRATES aircraft field campaign is provided in Section S1, with a list of in-situ probes and radar-lidar instruments onboard the research aircraft in Table S1 of the Supplementary. This study primarily utilized the measurements from two airborne in-situ probes—CDP (Lance et al., 2010; Faber et al., 2018) and 2D-S (Lawson et al., 2006, Wu and McFarquhar, 2019), along remote sensors— GV-HCR (NCAR/EOL HCR Team., 2014, Romatschke et al., 2021, Vivekanandan et al., 2015) and NCAR-HSRL (NCAR/EOL HSRL Team., 2012, Eloranta., 2005, Su et al., 2008), aboard the Gulfstream-V (GV) research aircraft during SOCRATES. The bulk cloud microphysical properties (LWC, particle size distributions, and number concentration) were derived from the CDP and 2D-S measurements, which were merged into a continuous dataset with size bins from 2 to 40 μm for cloud droplets and 40 to 1280 μm for drizzle particles, at 1 Hz temporal resolution for each flight. Following Zheng (2024), the CDP and 2D-S datasets were combined into a single size distribution, with droplet number concentrations in the overlapping size bin redistributed using a gamma distribution, ensuring a complete cloud and drizzle size spectrum.

The HCR reflectivity (dBZ), Doppler velocity (V_d) (m/s), and spectrum width (WID) (m/s) along with the HSRL measured backscatter coefficient (β) ($m^{-1}sr^{-1}$) and particle depolarization ratio (PLDR) were collected at 1 Hz temporal resolution. The HSRL signals are highly sensitive to cloud droplet concentrations and can be attenuated within a few hundred meters in liquid cloud layers (Ewald et al., 2021; Sassen, 1991). Estimated instantaneous uncertainties for HSRL measurements at 532 nm are 0.36 for backscatter (β) and 0.009 for depolarization (δ) (Su et al., 2008). Due to signal attenuation, HSRL detects fewer clouds than HCR, particularly in optically thick clouds. The radar-lidar overlap is about 11% when considering full time-height (3D) cloud profiles. Given this limitation, lidar signals are not used for phase or boundary estimation in optically thicker MBL clouds. Cloud temperatures were provided by the 2-dimensional ERA5 reanalysis product which matched the vertical and temporal resolution of the HCR data (NCAR/EOL HCR Team, 2023). The HCR dataset was further filtered to retain only nadir or zenith pointing observations, excluding all cloud samples in transition or rotational pointing directions (i.e., those not equal to ±90 degrees).

https://doi.org/10.5194/egusphere-2025-874
Preprint. Discussion started: 2 June 2025

2.2 Estimating LWC-Z relationship and LWP from in-situ measurements

The cloud-droplet number concentration and particle size distribution from the merged CDP+2D-S dataset is used to calculate in-situ reflectivity factor (Z, mm^6/m^3) and liquid water content (LWC, g/m^3) for cloud and drizzle particles, using the equations (Doviak et al., 1993; Kang et al., 2021; Zheng et al., 2024) as follows:

$$\boldsymbol{Z = \int_{D_{min}}^{\infty} N(D) D^6 dD} \quad (1)$$

$$\boldsymbol{LWC = \rho_w \frac{\pi}{6} \int_{D_{min}}^{\infty} N(D) D^3 dD} \quad (2)$$

where ρ_w is the density of liquid water, D is the particle diameter measured as droplet size distribution (DSD) from the CDP+2D-S particle size bins, and N(D) is the number concentration ($\#/cm^3$) per bin. Z (mm^6/m^3) can further be converted to dBZ as $dBZ = 10log(Z)$.

Clouds is defined when LWC is greater than 0.01 g/m^3 and cloud droplet number concentration (N_c) is greater than 5 cm^{-3} (Zheng et al., 2024). The LWC threshold ensures sufficient cloud density and number concentration while removing clear-sky conditions and aerosol noise. The number concentration of ice particles > 200 µm is very low (Zheng et al., 2024), suggesting most ice-phase particles fall below the 2D-S-defined 200 µm threshold for ice particle size distribution (Wu & McFarquhar, 2019).

The LWC can be further used to compute the column-integrated liquid water path (LWP, g/m^2) as a function of cloud layer thickness (Δh, meters) (Dong & Mace, 2002; Oh et al., 2018; Mioche et al., 2017), as follows:

$$\boldsymbol{LWP = \sum_{\{H_{base}\}}^{\{H_{top}\}} LWC(h).\Delta h} \quad (3)$$

A total of 62 in-situ aircraft profiles (ascending and descending) were constructed from 10135 CDP+2D-S DSD spectra at 1 Hz. From these, in-situ Z, LWC, and LWP were derived and presented in Fig. 1. The profiles were selected to represent uniform single layer low-level stratocumulus MBL clouds.

https://doi.org/10.5194/egusphere-2025-874
Preprint. Discussion started: 2 June 2025

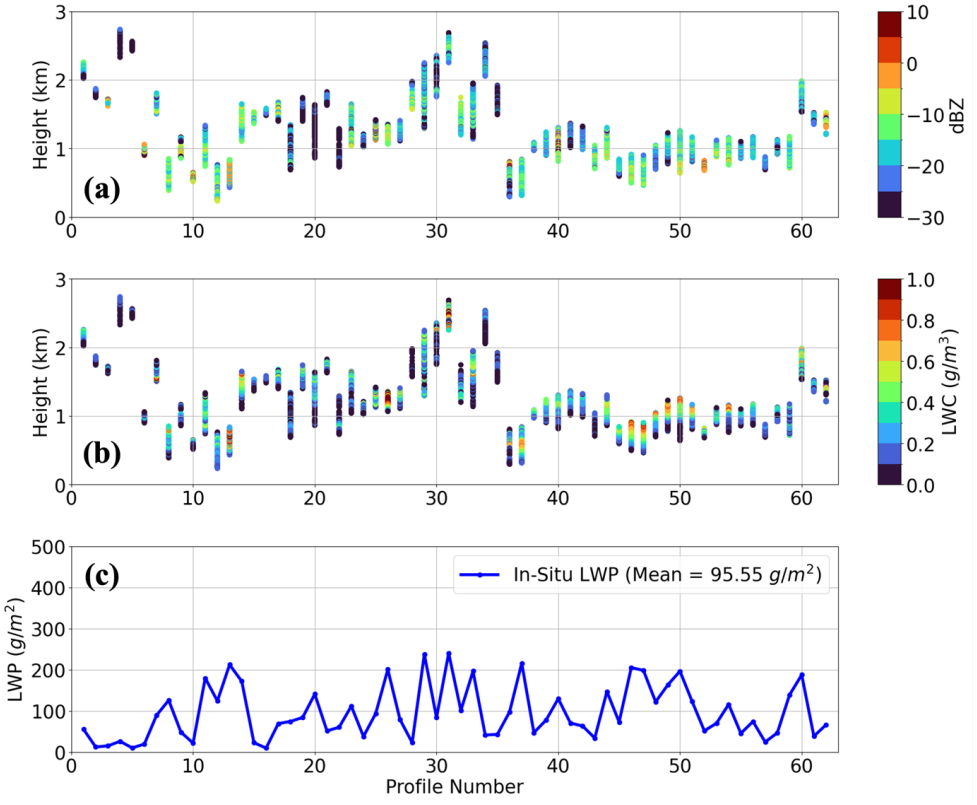

Figure 1. A total of 62 in-cloud profiles are composed from 10135 (1 Hz) SOCRATES CDP+2D-S DSD spectra to derive in-situ a) reflectivity profiles (Z was converted to dBZ) b) LWC (g/m^3) and c) LWP (g/m^2) as per equations 1, 2 and 3.

The in-situ measured LWC and Z can be used to derive an exponential relationship of form $\boldsymbol{LWC = aZ^b}$, where a, and b are intercept and slope parameters depending on cloud type (Oh et al., 2018). The in-situ Z and LWC measurements were constrained to only 5th to 95th percentile of the dataset to minimize the influence of extreme outliers. Furthermore, a kernel density estimation (KDE) was used to estimate relative point density in the Z-LWC (log) space. Due to the noisy nature of the dataset where larger particle diameters return extremely high Z values (~D^6) and relatively lower LWC values (~D^3), a log-log linear regression was performed only using a subset of the dataset with high sample density to minimize measurement uncertainties. An exponential relationship: $\boldsymbol{LWC = 0.70Z^{0.29}}$ is hence derived as shown in Fig. 2.

https://doi.org/10.5194/egusphere-2025-874
Preprint. Discussion started: 2 June 2025

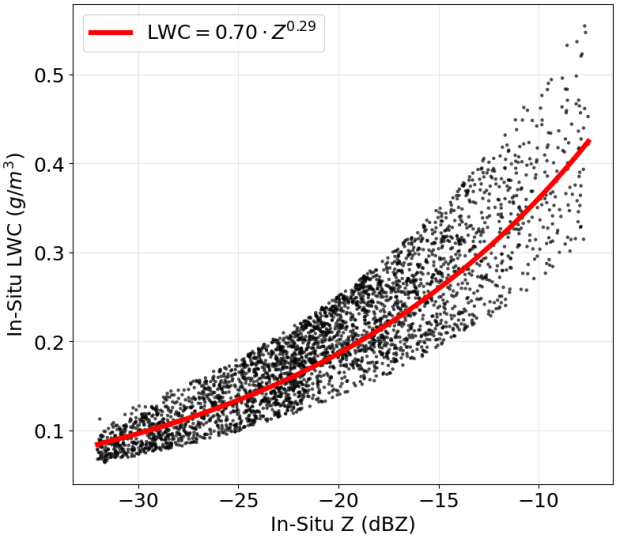

FIGURE 2. Exponential relationship between Z-LWC derived from the 10135 in-situ DSD measurements for the 62 in-cloud profiles from SOCRATES.

The predicted LWCs from the LWC-Z relationship are evaluated by against the in-situ measured LWCs for the 62 profiles of droplet spectra, with means of 0.21 g/m³ for predicted LWCs and 0.27 g/m³ for in-situ measurements. The root mean square error (RMSE) is approximately 0.03 g/m³. Furthermore, the predicted LWC profiles were used to estimate predicted LWPs using equation 3 which and against the 62 in-situ LWPs. The means of predicted and in-situ LWPs are 93.73 g/m^2 and 95.55 g/m^2, with an RMSE around 12 g/m^2.

The derived LWC-Z relationship, developed following existing studies like Oh (2018) and Vivekanandan (2020), is specifically tuned to low-level stratocumulus clouds sampled during the SOCRATES campaign but shall ideally be applicable to similar cloud cases for a range of W-band reflectivity profiles between -30 to 10 dBZ. Variations in the DSD contribute to uncertainties in cloud microphysical properties, which could impact the calculated reflectivity (Z) (Vivekanandan et al., 2020). Additionally, the presence of larger drizzle and precipitation particles is a major source of uncertainty in LWC-Z power-law relationships, thus it should be used with caution.

3 Classifying low-level clouds over SO

3.1 Identifying cloud boundaries using HCR measurements

Existing methods for estimating cloud-base (H_{base}) and cloud-top (H_{top}) heights, rely on the thresholds of lidar returned power, depolarization, or backscatter (e.g., Intrieri et al., 2002; Kang et al., 2021, 2024), as well as in-situ vertically resolved cloud LWP, LWC, and cloud-droplet number concentration (N_C). Kang (2024) presented a method using HSRL backscatter coefficient (β), where cloud base is defined as the first lidar range gate where $\beta > 10^{-4}$ m^{-1}sr^{-1}. This approach is effective when the aircraft is flying below the cloud base with radar-lidar pointed zenith. Similarly, HSRL signals can accurately detect cloud top when the aircraft is above the cloud with sensors pointing nadir. However, lidar alone cannot simultaneously estimate both cloud base and top heights, as HCR does. Therefore, only HCR measurements

https://doi.org/10.5194/egusphere-2025-874
Preprint. Discussion started: 2 June 2025

were used, which can determine cloud boundaries regardless of the aircraft's altitude or the pointing direction of the remote sensors.

In this study, H_{base} was estimated as the lowest height (from the sea surface) where the HCR Spectrum Width (WID) gradient has the lowest value (or highest negative gradient). The lowest WID gradient indicates the change from a precipitation layer to the cloud layer where the gradient of spectrum width decreases sharply. Higher spectrum width around the cloud base indicates a greater turbulence and wider range of particle velocities observed which correlate to potentially stronger turbulence, and likely drizzle or precipitation. The uncertainties arising from the low signal-to-noise ratios of radar signals near the ocean surface are effectively mitigated because this method only considers the cloud base after eliminating one or two lowest near-surface radar range-gates. H_{top} was estimated as the highest altitude where prominent HCR signals (dBZ > -50) were observed, following the method of Kang (2024). Cloud thickness (ΔH) was then calculated as the difference between cloud-top and cloud-base heights, $\Delta H = H_{top} - H_{base}$. Isolated cloud transects with shallow vertical heights and small horizontal extents were excluded from this study.

After estimating H_{base} and H_{top}, cloud types were categorized following the classification method of Xi et al. (2010). A single-layered cloud is defined as having no additional cloud layers above or below during the observed period. Based on this classification, the most common cloud type is found to be single-layered low-level clouds (LOW, $H_{top} \leq 3$ km), followed by middle above low clouds (MOL, $H_{base} < 3$ km, $H_{top} \leq 6$ km) and single-layered middle-level clouds (MID, $H_{base} > 3$ km, $H_{top} \leq 6$ km). Single or double-layered clouds with H_{base} and/or $H_{top} > 6$ km were rarely observed and were excluded to optimize statistical consistency and minimize errors. Only single-layered LOW clouds are considered in this study, which was the predominant cloud type during SOCRATES (~85% of total samples). Furthermore, for cases where cloud vertical columns were intersected by aircraft ascents or descents, HCR cannot reliably observe cloud top or base due to its fixed nadir or zenith-pointing configuration. As a result, only fully sampled cloud profiles—where both cloud base and top are simultaneously observed by the radar—were considered for boundary and phase estimation. Two selected cases of estimated H_{top} and H_{base} for LOW clouds is illustrated in Fig. 3.

3.2 Statistical results from prominent cloud types

The derived exponential relationship $LWC = 0.70Z^{0.29}$ was applied to the HCR-observed reflectivity measurements to retrieve a 2D time-height LWC profile and column integrated LWP. Figure 3 illustrates the estimated cloud boundaries, LWC profile and LWP for two selected cases. Figure 3a and 3e clearly shows the derived cloud boundaries and HCR reflectivity profiles. Thicker cloud layers exhibit larger radar reflectivities, which lead to higher estimated cloud LWCs and LWPs as shown in Figs. 3c, 3g, and Figs. 3d, 3h. respectively. LWC profiles basically follow adiabatic increasing from cloud base to upper levels, then decreasing near cloud top due to cloud-top entrainment. As mentioned in Section 2, the derived LWC and LWP values have differences of ~ 22.2% and 1.9%, respectively, compared to aircraft in-situ measurements.

https://doi.org/10.5194/egusphere-2025-874
Preprint. Discussion started: 2 June 2025

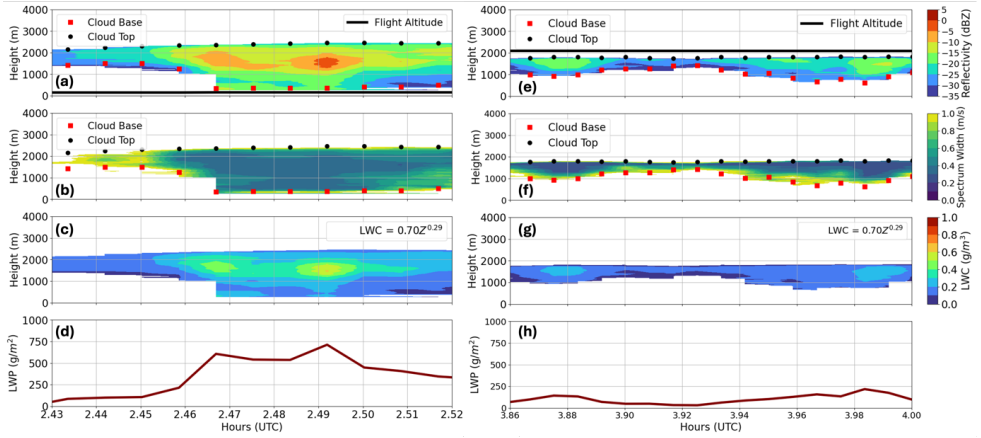

Figure 3. (a), (b), (c), and (d) are the profiles of HCR reflectivity (dBZ), spectrum width (m/s), LWC (g/m^3) and LWP (g/m^2), respectively for a selected case from RF1, while (e), (f), (g), (h) are similar profiles but from a selected case from RF7. The identified cloud top (black circles) and cloud base (red squares) heights have been illustrated along the HCR profiles along with the flight altitude (black line). The cases are selected such that the left panels represent the cloud profiles when the aircraft was flying above the cloud top (nadir-pointing radar), while the right panel shows a zenith-pointing radar cross-section with the aircraft flying below the cloud base. The time axis is in decimal hours (UTC).

LOW clouds were the most frequently observed cloud type—accounting for ~85% of occurrences across the 15 research flights during SOCRATES. In contrast, MID and MOL clouds were less common and together accounted for less than 15%, reflecting the SOCRATES campaign's sampling focus. Some rare occurrences of other high-altitude clouds were also identified but were excluded to maintain statistical consistency. These flights primarily sampled the cold sector of cyclones, occasionally crossing frontal systems associated with strong westerly winds over the Southern Ocean. The combination of large-scale weather patterns and a cool ocean surface led to persistent cloud cover, predominantly low- and mid-level stratus and stratocumulus clouds (McFarquhar et al., 2021; D'Alessandro et al., 2021).

The highest calculated LWP is associated with MOL clouds (~258 g/m²), followed by LOW (~133.2 g/m²) and MID (~48.3 g/m²) clouds, as presented in Table 1. The probability distribution histograms of LWP for the classified LOW, MID, and MOL clouds indicate significantly higher LWP values, with a notable frequency of LOW clouds exhibiting LWPs > 200 g/m². Another distinct peak corresponds to ice clouds with LWPs < 20 g/m². Despite this, overlaps are observed among the probability density functions (PDFs) of LWPs for the different cloud types.

The cloud LWP values during the Measurement of Aerosols, Radiation, and Clouds (MARCUS) ship-based field campaign (DeMott et al., 2018; Mace et al., 2021; McFarquhar et al., 2019, 2021; Marcovecchio et al., 2023; Xi et al., 2022) are retrieved using a physical-iterative algorithm applied to ship-based measurements of microwave radiometer (MWR) brightness temperatures at 23.8 and 31.4 GHz. These retrievals have associated uncertainties ranging from 15 to 30 g/m² (Caddedu et al., 2013), which align with the uncertainty estimates (~20 g/m²) of LWP retrievals obtained via statistical methods (Liljegren et al., 2001). Consequently, a threshold of 20 g/m² is employed in this study to distinguish between liquid clouds (LWP ≥ 20 g/m²) and ice clouds (LWP < 20 g/m²).

https://doi.org/10.5194/egusphere-2025-874
Preprint. Discussion started: 2 June 2025

Table 1. Mean, standard deviation, minimum, and maximum values for estimated cloud base and top heights, along with calculated LWP for each single-layered cloud type at a 30-second temporal average**.**

	LOW	MID	MOL
H_{base} ± SD	0.89 ± 0.61	3.97 ± 0.72	1.79 ± 0.86
Min, Max (km)	0.13, 2.95	3.01, 5.7	0.11, 2.95
H_{top} (mean) ± SD	1.70 ± 0.54	4.44 ± 0.80	4.10 ± 0.95
Min, Max (km)	0.30, 2.99	3.03, 5.91	3.01, 5.91
LWP (mean) ± SD (g/m^2)	133.17 ± 59	48.31 ± 29.4	257.95 ± 109

3.3 Evaluation and comparison of estimated cloud boundaries and LWPs

To evaluate the SOCRATES HCR-estimated boundaries, the H_{base} and H_{top} values were compared against those estimated by the Micropulse Lidar (MPL), Ceilometer, and 95 GHz W-band ARM Cloud Radar (WACR) measurements collected during the MARCUS campaign. These comparisons, conducted for low-level clouds within a spatiotemporally collocated region over the SO (Section S2, Fig. S1), revealed consistent patterns, as illustrated by the probability distribution function (PDF) histograms (Figs. 4a and 4b). The mean H_{base} (and H_{top}) height derived from SOCRATES HCR-profiles is ~0.89 km (~1.7 km) with average standard deviation around 0.55 km. While corresponding estimates from the MARCUS MPL/ceilometer are around ~0.93 km (~1.41 km) with standard deviation of around 0.58 km. The mean differences of H_{base} and H_{top} are ~0.04 km and ~0.29 km, respectively. Furthermore, HCR-derived H_{base} values were compared with those derived from GV-HSRL lidar observations for periods where the aircraft flew below the cloud base with a zenith-pointing radar-lidar view direction. The HSRL-detected H_{base} was identified as the first range gate where the backscatter coefficient (β) exceeded 10^{-4} $m^{-1}sr^{-1}$ (Kang et al., 2024). In these cases, which comprised ~20% of the total samples, both HCR and HSRL simultaneously detected cloud bases. A statistical comparison revealed a strong correlation of 0.78 ($p << 0.001$) and RMSE of 0.29 km (Fig. 4c). Notably, HSRL-retrieved H_{base} heights are consistently higher than those derived from HCR, by approximately 300-400 m.

Figure 4d presents PDFs comparing SOCRATES-derived LWP with MWR-retrieved LWP from the MARCUS campaign for LOW clouds, showing similar trends between the two datasets. The mean LWP derived from SOCRATES low clouds is 133.2 g/m^2, while MARCUS MWR yields a mean of 123.96 g/m^2. Overall, the statistical comparisons of H_{base}, H_{top}, and LWP for LOW clouds derived from the SOCRATES aircraft-based remote sensors demonstrate decent agreement with corresponding estimates from ship-based measurements during the MARCUS campaign, within the measurement uncertainties. The differences in observed measurements arise from the distinct (spatiotemporal) sampling strategies of the two campaigns which makes it difficult to obtain precisely overlapping cloud profile observations.

https://doi.org/10.5194/egusphere-2025-874
Preprint. Discussion started: 2 June 2025

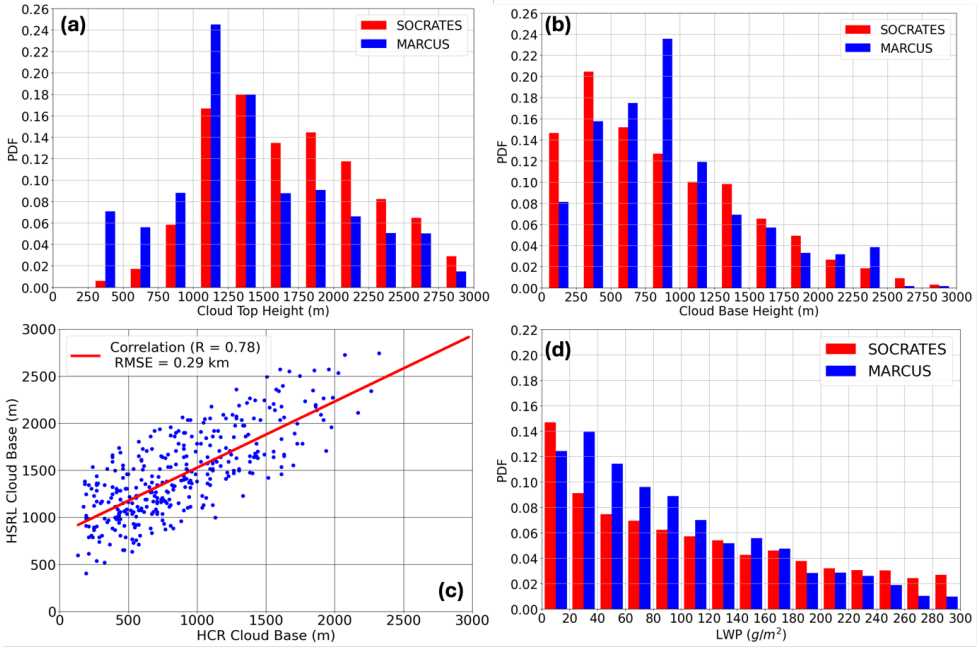

FIGURE 4. Comparison of the estimated cloud boundaries and LWP: Probability Density Function (PDF) histograms for (a) cloud base heights, and (b) cloud top heights derived from SOCRATES HCR- and MARCUS MPL/Ceilometer/WACR-measurements. (c) Cloud-base heights derived from SOCRATES HCR and HSRL measurements when the aircraft flew below the cloud base for all 15 research flights. (d) LWP comparison between SOCRATES and MARCUS MWR retrievals.4 Low-level cloud phase classification method and discussion

As discussed previously, LOW clouds are the dominant cloud type (~85%) observed during SOCRATES. This section outlines the method for determining LOW cloud phase.

4 Low-level cloud phase estimation

As discussed previously, LOW clouds are the dominant cloud type (~85%) observed during SOCRATES. This section outlines the method for determining LOW cloud phase. To ensure reliable phase classification, we exclude segments prone to high uncertainty, such as noisy pixels or very thin layers from steep sawtooth crossings and include only complete cloud profiles (as mentioned in Section 3.1).

4.1 Determination of cloud phase

Figure 5 presents the flowchart for determining cloud phase for the classified LOW clouds (H_{top} < 3 km) after applying the in-cloud condition constraint (LWC > 0.01 g/m³). The phase partitioning method is used as a set of combined filters, classifying cloud phase as a 2D profile of liquid, mixed, and ice phases. Additional cloud phase type classes, such as drizzle, rain, and snow are also classified. Phase classification is carried in a stepwise manner. The cloud phase classification in this study—based on profiles of air temperature (T), LWP, HCR reflectivity (dBZ), Doppler velocity (V_d), and Doppler spectrum width (WID), as described in Fig. 5—is

https://doi.org/10.5194/egusphere-2025-874
Preprint. Discussion started: 2 June 2025

performed in conjunction with the bivariate histograms presented in Fig. 6 for classifying liquid, mixed, ice, drizzle, rain and snow phase types. Because of overlapping constraints across multiple datasets, preserving the order of classification is important.

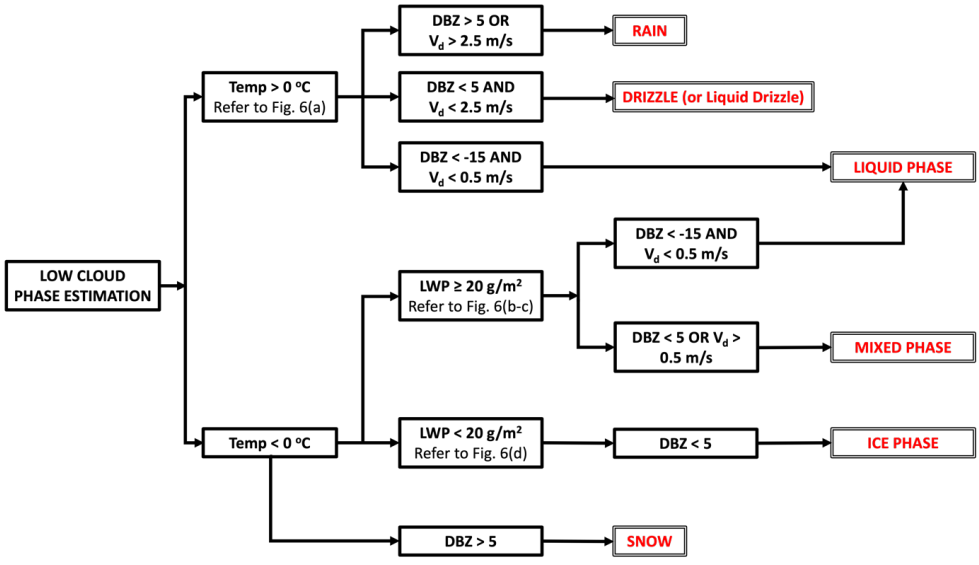

Figure 5. Flow chart depicting the phase classification of single-layered LOW clouds during SOCRATES. Temperature is provided from ERA5 reanalysis air temperature product.

Regions of strong precipitation are identified based on cloud profiles exhibiting strong HCR reflectivity (dBZ > 5), classified as rain in warm conditions (temperature, T > 0 °C) or snow in cold conditions (T<0 °C). Additionally, warm cloud regions (T > 0 °C) with extremely strong downdrafts (doppler velocity, V_d > 2.5 m/s) are also categorized as rain. Clouds with T > 0°C, dBZ < -15, and weak updraft (V_d < 0.5 m/s) are classified as liquid while drizzle typically has higher reflectivity (> -15 dBZ, Wu et al., 2020a) and V_d < 2.5 m/s (moderately strong downdraft/turbulence). Figure 6a presents the classification of hydrometeor types within warm cloud regions, distinguishing between liquid-phase clouds (dBZ ≤ 15, V_d < 0.5 m/s), drizzle (-15 < dBZ < 5 or V_d > 0.5 m/s), and rain (dBZ > 5). A clear linear relationship between V_d and dBZ is observed, with drizzle dominating the distribution, even in cases where dBZ < -15 and V_d > 0.5 m/s. These findings are consistent with Marcovecchio (2023), who reported a high drizzle frequency (71.8%) in MARCUS field campaign data.

As discussed in Section 3.2, a threshold of LWP = 20 g/m² is used to classify cloud phase: ice clouds (LWP < 20 g/m²) and mixed-phase or liquid clouds (LWP ≥ 20 g/m²), as illustrated in Fig. 5. The width of the Doppler spectrum (WID) serves as an indicator of cloud microphysical variability, with lower WID values suggesting homogeneous, single-phase clouds, and higher WID values indicating increased turbulence, wind shear, or mixed-phase conditions (Shupe, 2007). In subfreezing regions (T < 0°C), clouds characterized by low WID, and weak updrafts (V_d < 0.5 m/s) are classified as liquid, typically composed of small droplets and supercooled liquid water (SLW). Mixed-phase clouds are identified when both WID and V_d exceed 0.5 m/s, indicating greater turbulence and broader hydrometeor size distributions.

Clouds with WID > 0.5 m/s and V_d < 0.5 m/s (or vice versa) are reclassified based on reflectivity: as mixed-phase when dBZ > –15, and as liquid when dBZ < –15. Since radar

https://doi.org/10.5194/egusphere-2025-874
Preprint. Discussion started: 2 June 2025

reflectivity is proportional to the sixth power of particle diameter (Wang et al., 2009), clouds composed of small, uniform liquid droplets exhibit lower dBZ values, while mixed-phase clouds produce higher reflectivities due to the presence of larger particles. The classification of liquid and mixed-phase clouds under varying turbulence conditions is shown in Fig. 6b (WID > 0.5 m/s) and Fig. 6c (WID < 0.5 m/s). Most reflectivities fall below –15 dBZ, and a V_d–dBZ linear relationship, similar to that in Fig. 6a but with different slopes, is observed. The 2D distribution pattern in Fig. 6c resembles that of Fig. 6a, further supporting the dominance of drizzle in LOW clouds over the SO. Ice-phase regions (T < 0°C, LWP < 20 g/m²) are depicted in Fig. 6d, where ice is distinguished from snow in low-turbulence environments (WID < 0.5 m/s) by low reflectivity (dBZ < 5).

In regions where LWP ≥ 20 g/m², pixels with elevated LWCs (> 0.2 g/m³) are reclassified as pure liquid-phase clouds. Snow classification, presented in Figs. 6b–d, applies to all regions with T < 0°C. Where both LWP > 20 g/m² and subfreezing temperatures occur, precipitation may include supercooled (or freezing) rain in turbulent environments (WID > 0.5 m/s, Fig. 6b), or rimed snow and graupel in less turbulent settings (WID < 0.5 m/s, Fig. 6c). These regions are uniformly identified as snow, based on the assumption that supercooled precipitation freezes upon descent due to contact with airborne particles in downdrafts (Brownscombe & Hallett, 1967).

Although the phase-classification thresholds for WID, V_d, and dBZ were specifically tuned for clouds sampled during SOCRATES, we expect them to be broadly applicable to MBL clouds over the SO. To ensure consistency, the phase-diagnostic thresholds adopted in this study were compared with values reported in previous studies (e.g., Xi et al., 2022; Romatschke & Vivekanandan, 2022; Desai et al., 2023; Shupe, 2007). As Shupe (2007) noted, there are occasional cases where the applied V_d and WID thresholds may suggest a mixed or liquid phase even though ice is the dominant hydrometeor type at that altitude.

https://doi.org/10.5194/egusphere-2025-874
Preprint. Discussion started: 2 June 2025

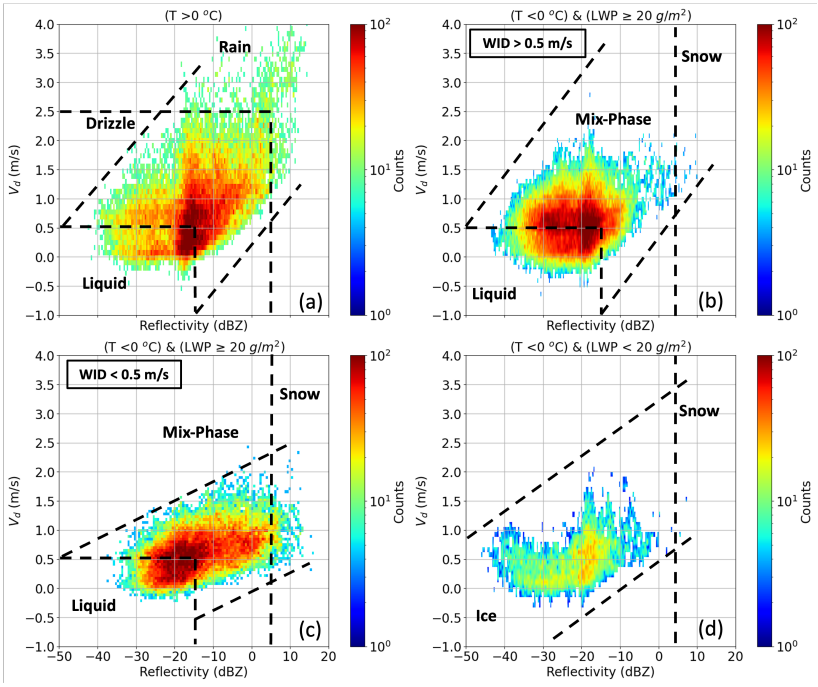

Figure 6. (a-d) Bivariate histograms of HCR reflectivity (dBZ) and Doppler velocity (V_d) for different spectrum widths (WID), LWP and temperatures (T) to demonstrate the classified liquid, ice and mixed phase cloud samples. The colorbar shows the sample count in each bin in a log-scale and the dashed lines represent the threshold values for the phase classification. The phase class types of rain, drizzle, and snow are also classified.

4.2 Results for LOW cloud phase classification

An LWP greater than the retrieval uncertainty (≥ 20 g/m^2) indicates the presence of liquid water (at T> 0 ºC) or supercooled liquid water (SLW, at T < 0 ºC). Larger ice particles, being denser than liquid droplets, typically exhibiting broader Doppler spectrum widths and higher fall speeds (Xi et al., 2022). A significant number of drizzle (at T > 0 ºC) and mixed-phase (T < 0 ºC) samples were observed near cloud base, likely driven by elevated WID and V_d values. Mixed-phase clouds represent a complex three-phased colloidal system in which SLW droplets coexist with ice crystals, influencing both the nature of mixed-phase layers (genuinely and/or conditionally mixed) and underlying microphysical processes (Korelov & Milbrandt, 2022; Maciel et al., 2024). D'Alessandro (2021) found that SO clouds sampled during SOCRATES exhibited significant spatial heterogeneity. Low-level clouds generally exhibit higher temperatures than recorded aircraft temperatures due to altitude differences between flight paths and cloud boundaries. Analyzing the ERA5 air temperature indicates that mode temperatures ranged between -5°C and 0°C for all three phases (liquid, mixed and ice). Notably, mixed-phase clouds show the highest occurrence between -15°C to -2.5°C, underscoring the spatial heterogeneity of low-level stratocumulus clouds, consistent with the findings from D'Alessandro (2021) and Maciel (2024).

Based on a 30-second temporal averaging interval, the classification method developed in this study identified liquid-phase clouds, including SLW, as the most frequent category, accounting for 48.79% of all samples. Mixed-phase and ice-phase clouds comprised 23.26% and 6.88%, respectively. Increasing the temporal averaging interval results in a higher

https://doi.org/10.5194/egusphere-2025-874
Preprint. Discussion started: 2 June 2025

proportion of mixed-phase clouds and a corresponding decrease in the occurrence of single-phase clouds. Drizzle was identified in 16.22% of the cases, while rain (3.35%) and snow (1.51%) were relatively rare. Most of the rain and snow detections correspond to in-cloud precipitation, with some falling hydrometeors observed near cloud base.

Figure. 7a–e illustrates the profiles for HCR-dBZ, WID, V_d, LWC and LWP for a flight case (RF13), with Fig. 7f showing the resulting classified phases. Notably, regions where mixed-phase layers overlay liquid-only columns suggest cloud-top entrainment. In these cases, mixing of dry air into the cloud top enhances evaporation of liquid droplets, promoting the formation of mixed-phase conditions. Analysis of 2D-S particle probe imagery (Wu and McFarquhar, 2019) reveals that liquid droplets are predominantly spherical, whereas large ice particles display irregular morphologies. While large ice particles (D_p > 200 μm) can be visually identified by shape, small ice crystals are not well-resolved by the 2D-S probe, making it difficult to distinguish them from similarly sized cloud droplets.

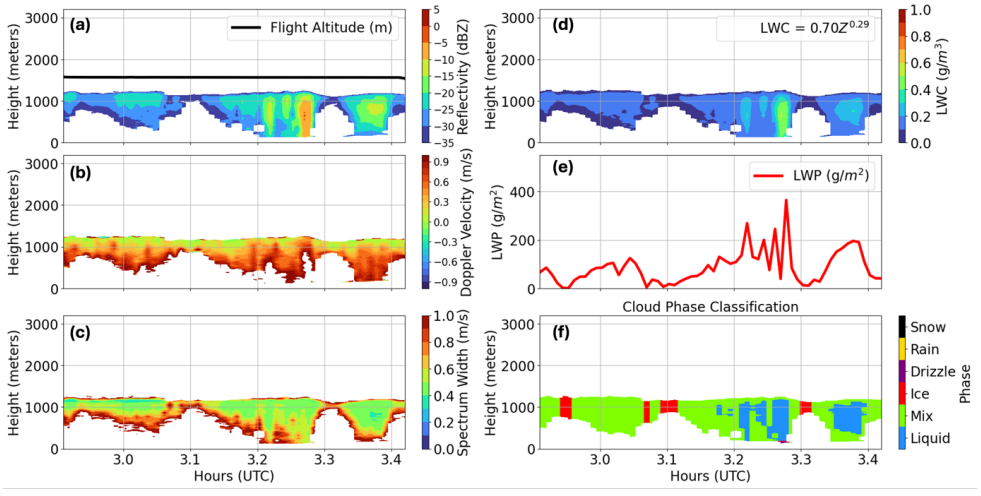

Figure 7. A case study from SOCRATES flight RF13 illustrating the phase-classification algorithm. Shown are: (a) HCR reflectivity (dBZ) with the flight altitude (black line), (b) Doppler velocity (V_d), and (c) Doppler spectrum width (WID) profiles. (d) LWC profile (retrieved from HCR reflectivity), (e) column-integrated LWP, and (f) classified cloud phase categories. The time axis is in decimal hours (UTC).

4.3 Evaluation of phase-classification with existing methods

Cloud phase classification is highly sensitive to observational scales, sampling strategy, and instrumentation type. This study focuses exclusively on low-level SO clouds observed during SOCRATES. The phase-classification method developed here (hereinafter referred to as HCR-phase) is evaluated through comparisons with five existing methodologies, grouped into three categories: 1) machine learning methods based on in-situ probes — this includes multinomial logistic regression (MLR) (D'Alessandro et al., 2021; Schima et al. 2022) and the University of Washington Ice–Liquid Discriminator (UWILD) (Atlas et al., 2021); 2) ship-based radar-lidar-MWR measurements from MARCUS (Xi et al., 2022; Zhang and Levin, 2017) ; 3) fuzzy logic particle identification (PID) — developed from airborne HCR and HRSL measurements during SOCRATES (Romatschke and Vivekanandan, 2022). Only low-level cloud samples below 3km were used for cross-method comparisons. The comparative analysis aims to assess

https://doi.org/10.5194/egusphere-2025-874
Preprint. Discussion started: 2 June 2025

the strengths and limitations of the HCR-phase classification in the context of these existing methodologies.

4.3.1 Comparison with in-situ phase classification (machine learning methods: MLR and UWILD)

D'Alessandro (2021) developed a cloud phase classification method using an MLR model trained on in-situ measurements from the CDP, 2D-S, and Rosemount Icing Detector (RICE) collected during the SOCRATES campaign. This model classified cloud phase—liquid, mixed, or ice—for samples at air temperatures below 0°C. Schima (2022) refined the MLR product by manually evaluating imagery from the 2D-S, 2D-C, and PHIPS (Particle Habit Imaging and Polar Scattering) probes. Among 1600 in-situ samples collected below 3 km altitude, the MLR approach classified 52.25% as liquid, 9.5% as mixed-phase, and 38.2% as ice clouds. Approximately, 39% of samples at temperatures above freezing ($T > 0°C$) remain unclassified; including these would likely raise the overall fractions of liquid and mixed-phase clouds in the MLR dataset. Compared to the HCR-phase method developed in this study, the MLR model detects a larger fraction of liquid clouds but underrepresents mixed-phase and ice clouds.

HCR-phase classification was also compared with the UWILD product, which uses a random forest algorithm trained on 2D-S probe images and particle inter-arrival times (Atlas et al., 2021; Mohrmann et al., 2021), and validated with PHIPS imagery. For consistency, UWILD timestamps with nearly equal liquid and ice samples were reclassified as mixed phase. Among time periods overlapping with HCR-phase (matched to the nearest second), UWILD classified 58.8% of samples as liquid, 38.9% as mixed-phase clouds, and only 2.3% as ice-phase clouds. Increasing the temporal averaging interval led to a higher frequency of mixed-phase classification (77%), with reduced occurrences of liquid (19%) and ice (4%). A key source of uncertainty arises from the spatial heterogeneity of clouds and the UWILD algorithm's lack of an explicit mixed-phase category. Additionally, UWILD defines all small particles (equivalent diameter $D_{eq} < 0.17$ mm) as liquid, which likely underrepresents ice-phase clouds. This limitation is significant, as the SOCRATES campaign sampled very few particles larger than 0.17 mm, even within clouds confirmed to be in the ice phase (Zheng et al., 2024; Wu and McFarquhar, 2019).

Within the same samples, the HCR-phase method classified 61.81% of samples as liquid, 29.47% as mixed-phase clouds, and 8.71% as ice-phase clouds. A key challenge in comparing in-situ ML-based phase classifications with the HCR-phase method lies in the differing observational frameworks. Both the MLR and UWILD classifiers are trained on microphysical probe data (e.g., CDP and 2D-S) collected at the GV aircraft's altitude, and therefore cannot provide phase information across the full vertical extent of HCR-observed cloud profiles. This limitation is especially pertinent when the aircraft is flying above or below cloud layers. Furthermore, the MLR algorithm is specifically designed for classifying cloud phases under subfreezing conditions, making it most applicable to cold cloud environments. A substantial number of unclassified points—particularly those at temperatures above 0°C—are excluded from final phase statistics, further complicating direct, one-to-one comparisons. Nevertheless, this comparison does provide a valuable approximation of how in-situ measured cloud phases compares to HCR-derived cloud phases.

4.3.2 Comparison with ship-based phase classification during MARCUS

The HCR-phase classification was further evaluated through comparison with single-layer, low-cloud (<3 km) phase classifications from the ship-based measurements during the

https://doi.org/10.5194/egusphere-2025-874
Preprint. Discussion started: 2 June 2025

MARCUS campaign, focusing on a spatiotemporally collocated region over the SO using a 5-minute averaging interval (see Section S2). Zhang and Levin (2017) developed the thermodynamic cloud phase product (THERMOCLDPHASE; ARM, 2017) for MARCUS using data from the U.S. DOE's ARM Mobile Facility deployed aboard the *Aurora Australis*. This product integrates active remote sensing instruments—including the Micropulse Lidar (MPL) and W-band ARM Cloud Radar (WACR)—with passive sensors such as microwave radiometers (MWR) and radiosondes. Cloud phase classification is based on the Shupe (2005, 2007) methodology and includes seven thermodynamic hydrometeor types. More recently, Xi (2022) introduced an improved classification approach tailored to single-layer low-level clouds over the SO, leveraging WACR Doppler spectra, MWR-derived LWP, and radiosonde-based temperature profiles.

For a total of 1410 5-min samples, Xi (2022) classified 58.6% as liquid-phase, 30.7% as mixed-phase, and 10.6% as ice-phase clouds. In contrast, the thermodynamic cloud phase product (ARM, 2020) identified 52.31% liquid, 25.15% mixed, and 22.53% ice-phase clouds across 3435 samples. The statistical results from both these methods remain broadly consistent within the same phase categories with those obtained using the HCR-phase classification (61.81% liquid, 29.47% mixed-phase, and 8.71% ice; excluding drizzle, rain, and snow). The differences in the phase partitioning are expected, given the inherent limitations in achieving perfect spatiotemporal alignment between the SOCRATES and MARCUS campaigns.

4.3.3 Comparisons with fuzzy logic particle identification (PID)

Romatschke and Vivekanandan (2022) developed a technique for identifying hydrometeor particle types using HCR and HSRL observations during the SOCRATES campaign. A fuzzy logic particle identification (PID) algorithm was developed using HCR, HSRL, and temperature parameters (NCAR/EOL HCR Team, 2023) to classify 11 distinct hydrometeor types. This PID dataset served as a valuable reference for validating the HCR-phase classification through a pixel-by-pixel comparison for low-level clouds, using a 10-second temporal average. To ensure consistent comparisons, the PID-classified 'cloud liquid' and 'supercooled cloud liquid' categories were merged into a single 'cloud liquid' category, while categories such as 'supercooled drizzle' and 'supercooled rain' were excluded due to their minimal sample counts. Table 2 summarizes the raw sample (pixel) counts for each phase category, comparing results between the HCR-phase classification and the PID-derived hydrometeor types.

Table 2. Comparison of HCR-phase classification and PID at a 30-second temporal resolution.

Numbers represent pixel counts		PID Scheme							
		Cloud	Precipitation	Small Frozen	Large Frozen	Melting	Cloud Liquid	Drizzle	Rain
HCR-Phase	Liquid	54114	563	4135	760	178	20084	6	0
	Mix	19448	182	754	18	2	13784	0	0
	Ice	8039	59	270	33	2	2902	0	0
	Drizzle	2115	25	149	40	590	3614	17814	0
	Rain	245	3	0	88	614	589	2612	1326
	Snow	22	30	68	2115	31	6	5	0

Figure 8 illustrates the distribution of PID-scheme phase categories corresponding to each HCR-phase, based on overlapping pixels where both methods provide valid results. For

https://doi.org/10.5194/egusphere-2025-874
Preprint. Discussion started: 2 June 2025

these matched samples, the HCR-phase classification identifies cloud and in-cloud precipitation hydrometeor types as approximately 64.4% (65.3%) liquid, 23.2% (21.1%) mixed-phase, and 9.6% (6.8%) ice-phase. Notably, 69.3% of the large frozen hydrometeor types from the PID are classified as snow in the HCR-phase, reflecting the threshold-based classification scheme used in this study, which tends to identify large ice particles with high reflectivity (dBZ) and low LWP as snow. Similarly, PID-classified drizzle is mapped to 87.2% drizzle and 12.8% rain in HCR-phase, while all PID-classified rain is consistently identified as rain by HCR-phase. The melting layer observed in MBL clouds, characterized by enhanced dBZ values similar to drizzle, contains both liquid and ice-phase particles as hydrometeors melt while falling through the 0°C isotherm (Song et al., 2021). Accordingly, HCR-phase classifies PID melting layer samples as 41.6% drizzle, 43.3% in-cloud rain, and 12.6% liquid clouds.

The greatest mismatch occurs for PID-classified small frozen hydrometeors, which are identified as 76.9% liquid, 14% mixed-phase, and only 5% ice by the HCR-phase method. This discrepancy likely reflects the presence of supercooled liquid droplets coexisting with ice particles, which HCR-phase identifies using its criteria of low dBZ, V_d, and high LWP; while the PID algorithm do not use any LWP constraints. Among the matched samples, PID-classified 'cloud liquid' (merged with 'supercooled cloud liquid') types account for 49% of HCR-phase liquid and 33.6% of mixed-phase classifications. These percentages are derived from the subset of low-level clouds with collocated pixels and do not represent the full PID dataset.

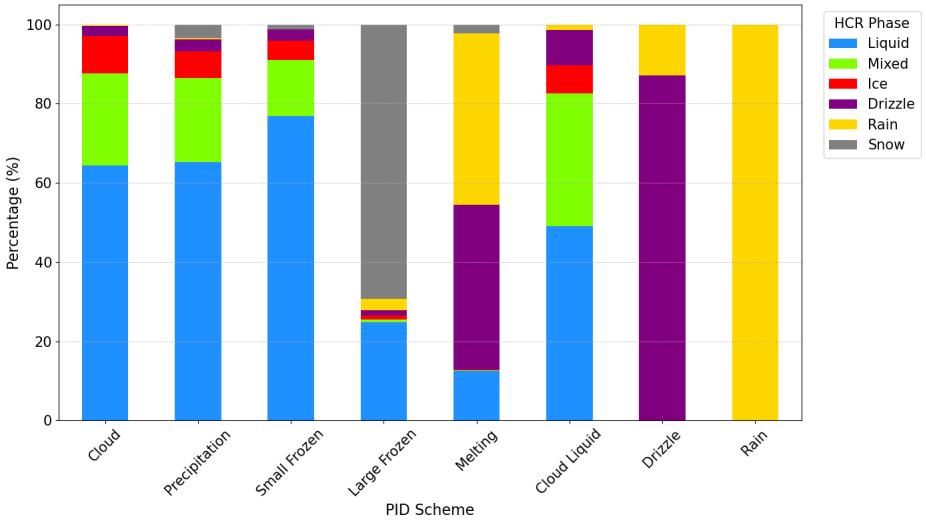

Figure 8. The distribution of phase partitioning of hydrometeor types identified by the PID algorithm, showing the percentages of each phase-category samples as per the overlapping pixels with HCR-phase.

4.4 Summarizing the comparisons between HCR-phase and other methods

Table 3(a,b) summarizes the low-level cloud phase classifications from the HCR-phase algorithm alongside results from five other methods. For the SOCRATES campaign, comparisons include the MLR method (Schima, 2022; D'Alessandro, 2021, 2022), and the fuzzy logic PID algorithm (Romatschke and Vivekanandan, 2022). For the MARCUS campaign, comparisons are made with WACR-MWR retrievals (Xi et al., 2022) and the Thermodynamic Cloud Phase product (ARM, 2017).

https://doi.org/10.5194/egusphere-2025-874
Preprint. Discussion started: 2 June 2025

The MLR method predicts 9.6% fewer liquid-phase clouds, 20% fewer mixed-phase, and 29.5% fewer ice-phase clouds compared to the HCR-phase (Table 3a, column 2). Additionally, ~39% of the MLR samples are unclassified in regions exceeding 0°C; which were excluded from the comparison. In contrast, UWILD results show closer agreement with HCR-phase, with only a 3% difference in liquid-phase occurrence. However, UWILD reports 9.4% more mixed-phase and 6.4% fewer ice-phase clouds (Table 3a, column 3). For the MARCUS campaign, the Xi (2022) phase classification method aligns closely with HCR-phase, underestimating liquid-phase clouds by just 3.2% and differing by only 1.2% and 1.9% in mixed and ice phases, respectively (Table 3a, column 5). Similarly, the Thermodynamic Cloud Phase product identifies 7.3% more ice-phase clouds, but 2.3% fewer liquid and 5% fewer mixed-phase clouds relative to HCR-phase. Table 3b compares the HCR-phase results with the fuzzy logic PID scheme. The PID method classifies 56.5% of matched low-level samples as liquid (including supercooled liquid) and 11.6% as frozen (large and small frozen hydrometeors), which is 7.7% higher in liquid and 3.2% higher in frozen phase (ice and snow samples) occurrence than HCR-phase. Additionally, PID estimates 11.9% more drizzle and 1.52% less rain compared to HCR-phase, highlighting notable differences in hydrometeor subtype identification.

Overall, the phase classification percentages show reasonable agreement across all methods, with the MLR method displaying the largest deviations. Mixed-phase cloud identification remains the most uncertain, particularly in regions with high spatial heterogeneity. The HCR-phase method, which combines radar observations with in-situ measurements, demonstrates strong capability in detecting mixed-phase clouds due to two primary factors: (1) the integrated use of HCR reflectivity (dBZ), spectral width (WID), and Doppler velocity (V_d) effectively characterizes particle size distributions, enabling clear differentiation between mixed-phase, drizzle, liquid, and ice clouds; and (2) the use of a 20 g/m² liquid water path (LWP) threshold helps distinguish ice-dominated columns from liquid and mixed-phase cloud regions.

Table 3. (a) Comparison of HCR-phase classification with in-situ ML phase products (MLR, UWILD) and MARCUS-phase retrievals. For HCR-phase, drizzle, rain, and snow categories are excluded from this comparison. (b) Comparison of HCR-phase with PID scheme. Frozen categories combine ice and snow (for HCR-phase), large frozen and small frozen (for PID).

(a)	Results from SOCRATES			Results from MARCUS	
	HCR-Phase	MLR	UWILD	WACR-MWR	Thermo-cloud phase
Liquid %	61.81	52.25	58.8	58.65	56.82
Mix %	29.47	9.50	38.9	30.71	27.2
Ice %	8.71	38.25	2.3	10.64	15.98

(b)	HCR-Phase	PID-scheme
Liquid %	48.79	56.45
Mix %	23.26	-
Melting %	-	1.95
Frozen %	8.39	11.61
Drizzle %	16.22	28.15
Rain %	3.35	1.83

https://doi.org/10.5194/egusphere-2025-874
Preprint. Discussion started: 2 June 2025

The percentage agreement for each phase is calculated by comparing the results from this study with those from the other methods. Agreement is defined as:

Agreement (%) = 100 - |(Phase$_i$% from compared method) - (Phase$_i$% from HCR-phase)|,

where i represents the phase categories.

Results show that the MLR method has the lowest agreement with HCR-phase for the mixed (80%) and ice (70.5%) phase categories, although it performs well for liquid clouds (90.4%). In contrast, the UWILD, WACR-MWR, and thermodynamic cloud phase methods exhibit strong agreement with HCR-phase, with >90% consistency across all three phase categories. The PID scheme also shows high agreement (~92.3%) with HCR-phase for liquid, frozen, drizzle, and rain categories. As previously discussed, the underlying differences between these classification methods - in terms of sensor type, sampling strategy, and algorithm design - contribute to the observed deviations. While direct one-to-one comparisons are inherently limited by methodological differences, these analyses offer a robust foundation for evaluating phase classification accuracy and consistency across platforms.

5 Summary and Conclusions

This study presents a comprehensive methodology for identifying cloud boundaries and classifying cloud phases in single-layer low-level marine boundary layer (MBL) clouds. The approach leverages data from the airborne HCR radar and in-situ cloud and drizzle probes (CDP and 2D-S) aboard the NSF/NCAR GV aircraft during SOCRATES campaign over the SO. Cloud base detection is achieved using the Doppler spectrum width gradient, which reliably identifies cloud boundaries even in the absence of supporting sonde or ceilometer measurements. The cloud phase classification (referred as HCR-phase), integrates radar observations with in-situ measurements, enabling accurate phase retrieval in the time-height dimension. In addition, the study provides some new insights into the macrophysical properties of different cloud types and phases through statistical analyses. Both the cloud base detection and phase classification methodologies were rigorously evaluated against existing methods. The major takeaways from this study are as follows:

1. A method based on HCR-reflectivity and spectrum width gradient-based method was used to identify cloud boundaries and classify cloud types into LOW, MID, and MOL categories, based on cloud-top and cloud-base heights. LOW clouds (< 3km) were the most frequently observed, occurring in 85% of observed cases. HCR- and HSRL-derived cloud base heights showed strong agreement, with a correlation of 0.78. PDFs of cloud base and top heights from SOCRATES (HCR) and MARCUS (MPL/ceilometer/WACR) over a collocated region also exhibited close agreement, with mean differences of 0.04 km for cloud base and 0.29 km for cloud top.
2. In-situ measured LWC and calculated reflectivity (Z) from CDP and 2D-S probe measurements were used to derive an empirical exponential relationship: LWC = $0.70Z^{0.29}$. This relationship was applied to HCR-reflectivity data to retrieve vertical LWC profiles over time. Using these LWC profiles and cloud thickness, LWP was estimated for each cloud category, with an associated uncertainty of approximately ±20 g/m². The mean LWP values were 133.2 g/m² for LOW clouds, 258 g/m² for MOL clouds, and 48.3 g/m² for MID clouds. Additionally, LWP estimates for SOCRATES low clouds were in close agreement with microwave radiometer (MWR)–retrieved LWP values from MARCUS, showing a mean difference of just 9.24 g/m².
3. A phase classification method (HCR-phase) was developed to categorize single-layered low-level (LOW) clouds into liquid, mixed, and ice phases, with respective occurrence frequencies of 48.8%, 23.3%, and 6.9%. Additional hydrometeor types, including

https://doi.org/10.5194/egusphere-2025-874
Preprint. Discussion started: 2 June 2025

drizzle (16.2%), rain (3.4%), and snow (1.5%), were also identified. The HCR-phase classifications were benchmarked against five existing methods: MLR, UWILD, PID, WACR-MWR, and Thermodynamic Cloud Phase. Overall, HCR-phase showed strong agreement (>90%) with these methods across the primary phase categories. The largest deviation was observed with the MLR method, which showed lower agreement (~70%) for mixed and ice phases, primarily due to methodological differences in classification criteria.

This study advances our understanding of Southern Ocean clouds by introducing robust methodologies for identifying cloud boundaries and classifying cloud phases in MBL clouds. The techniques developed here are broadly applicable to future field campaigns and research efforts aimed at characterizing MBL cloud properties in other remote maritime regions. A promising avenue for future investigation lies in the integration of HCR and HSRL observations which has significant potential in improving cloud phase and microphysical property retrievals. Further work may focus on refining the cloud boundary and phase classification algorithms, incorporating additional remote sensing instruments, and assessing the implications of cloud phase heterogeneity on aerosol–cloud–radiation interactions.

Data Availability. All radar-lidar and in-situ data from the NSF SOCRATES campaign used in this study are freely available via the EOL data archive (https://data.eol.ucar.edu/dataset/) and the SOCRATES website (https://www.eol.ucar.edu/field_projects/socrates). The 2D-S dataset (Wu & McFarquhar, 2019) is available at https://doi.org/10.26023/8HMG-WQP3-XA0X, and CDP data (UCAR/NCAR-EOL, 2022) at https://doi.org/10.5065/D6M32TM9. The MLR cloud phase dataset (D'Alessandro et al., 2021) can be found at https://doi.org/10.26023/S6WS-G5QE-H113 (https://data.eol.ucar.edu/dataset/552.142), and UWILD phase classification (Mohrmann et al., 2021) at https://doi.org/10.26023/PA5W-4DRX-W50A (https://data.eol.ucar.edu/dataset/552.134). NCAR HCR radar and GV-HSRL lidar moments data (NCAR/EOL HCR Team, NCAR/EOL GV-HSRL Team, 2023), including the fuzzy logic PID scheme (Romatschke & Vivekanandan, 2022), are available at https://doi.org/10.5065/D64J0CZS (https://data.eol.ucar.edu/dataset/552.034). Additional datasets, including ARM MWRRET1LILJCLOU, ARSCLWACRBND1KOLLIASSHP, and THERMOCLDPHASE for the MARCUS campaign, can be accessed via the ARM data store at https://adc.arm.gov/.

Author contributions. The idea of this study was discussed by AD, BX, and XD. AD performed the analyses and wrote the paper. AD, BX, XD, and XZ participated in the scientific discussions and provided substantial comments and edits on the paper.

Competing interests. The contact author has declared that neither they nor their co-authors have any competing interests.

Acknowledgments. The SOCRATES aircraft dataset, campaign details, and related publications are freely available at https://www.eol.ucar.edu/field_projects/socrates. We thank John D'Alessandro (University of Washington) for guidance on the MLR phase determination method, Ulrike Romatschke (NCAR) for explaining radar-lidar fuzzy logic parameters, and Christopher J. Webster (NCAR) for assistance with XPMS2D software. This manuscript was proofread using ChatGPT and Grammarly.

Financial Support. This work was supported by the University of Arizona's IT4IR TRIF and Provost Investigation funds. The researchers at the University of Arizona were also supported by NSF grant AGS-2031750 at the University of Arizona. The work at Argonne National

https://doi.org/10.5194/egusphere-2025-874
Preprint. Discussion started: 2 June 2025

Laboratory was supported by the U.S. DOE Office of Science under contract DE-AC02-06CH11357.

References

Atlas, R., Mohrmann, J., Finlon, J., Lu, J., Hsiao, I., Wood, R., & Diao, M.: The University of Washington Ice-Liquid Discriminator (UWILD) improves single-particle phase classifications of hydrometeors within Southern Ocean clouds using machine learning, Atmospheric Measurement Techniques, 14(11), 7079–7101, https://doi.org/10.5194/amt-14-7079-2021, 2021.

Atmospheric Radiation Measurement (ARM) user facility: Marine W-band ARM Cloud Radar, Active Remote Sensing of Clouds (ARSCLWACRBND1KOLLIASSHP), 2018-01-01 to 2018-03-24, ARM Mobile Facility (MAR) Hobart, AUS to Antarctic Coast – resupply ship Aurora Australis; AMF2 (M1), compiled by M. Wang and K. Johnson, ARM Data Center [data set], http://dx.doi.org/10.5439/1498737, 2017.

Atmospheric Radiation Measurement (ARM) user facility: MWR Retrievals (MWRRET1LILJCLOU), 2018-01-01 to 2018-03-23, ARM Mobile Facility (MAR) Hobart, AUS to Antarctic Coast – resupply ship Aurora Australis; AMF2 (M1), compiled by D. Zhang, ARM Data Center [data set], http://dx.doi.org/10.5439/1027369, 2017.

Atmospheric Radiation Measurement (ARM) user facility: Thermodynamic cloud phase (THERMOCLDPHASE), 2018-01-01 to 2018-03-24, ARM Mobile Facility (MAR) Hobart, AUS to Antarctic Coast - resupply ship Aurora Australis; AMF2 (M1), compiled by D. Zhang and M. Levin, ARM Data Center [data set], DOI:10.5439/1871014, 2017.

Baker, B., Mo, Q., Lawson, R. P., O'Connor, D., & Korolev, A.: Drop Size Distributions and the Lack of Small Drops in RICO Rain Shafts, J. Appl. Meteor. Climatol., 48, 616–623, https://doi.org/10.1175/2008JAMC1934.1, 2009.

Bodas-Salcedo, A., Hill, P. G., Furtado, K., Williams, K. D., Field, P. R., Manners, J. C., et al.: Large contribution of supercooled liquid clouds to the solar radiation budget of the Southern Ocean, Journal of Climate, 29(11), 4213–4228, https://doi.org/10.1175/JCLI-D-15-0564.1, 2016.

Brownscombe, J. L., & Hallett, J.: Experimental and field studies of precipitation particles formed by the freezing of supercooled water. Quarterly Journal of the Royal Meteorological Society, 93(398), 455-473, 1967.

Cadeddu, M. P., Liljegren, J. C., & Turner, D. D. (2013). The Atmospheric Radiation Measurements (ARM) program network of microwaveradiometers: Instrumentation, data, and retrievals. *Atmospheric Measurement Techniques*, *6*(9), 2359–2372. https://doi.org/10.5194/amt-6-2359, 2013.

D'Alessandro, J. J., Diao, M., Wu, C., Liu, X., Jensen, J. B., & Stephens, B. B.: Cloud phase and relative humidity distributions over the Southern Ocean in austral summer based on in situ observations and CAM5 simulations, Journal of Climate, 32(10), 2781–2805, https://doi.org/10.1175/JCLI-D-18-0232.1, 2019.

D'Alessandro, J. J., McFarquhar, G. M., Wu, W., Stith, J. L., Jensen, J. B., & Rauber, R. M.: Characterizing the Occurrence and Spatial Heterogeneity of Liquid, Ice, and Mixed Phase Low-Level Clouds Over the Southern Ocean Using in Situ Observations Acquired During SOCRATES, Journal of Geophysical Research: Atmospheres, 126(11), https://doi.org/10.1029/2020JD034482, 2021.

https://doi.org/10.5194/egusphere-2025-874
Preprint. Discussion started: 2 June 2025

D'Alessandro, J., Schima, J., McFarquhar, G.: SOCRATES Cloud Phase Product. Version 1.0. UCAR/NCAR - Earth Observing Laboratory [data set], https://doi.org/10.26023/S6WS-G5QE-H113, 2022.

Desai, N., Diao, M., Shi, Y., Liu, X., & Silber, I.: Ship-Based Observations and Climate Model Simulations of Cloud Phase Over the Southern Ocean, Journal of Geophysical Research: Atmospheres, 128(11), https://doi.org/10.1029/2023jd038581, 2023.

DeMott, P. J., Hill, T. C. J., and McFarquhar, G.: Measurements of aerosol radiation and clouds over the Southern Ocean (MARCUS) ice nucleating particle measurements field campaign report, U.S. Department of Energy, available at: https://www.osti.gov/servlets/purl/1489372, 2018.

Dong, X., Ackerman, T. P., and Clothiaux, E. E.: Parameterizations of the microphysical and shortwave radiative properties of boundary layer stratus from ground-based measurements, J. Geophys. Res., 103, 31681–31693, https://doi.org/10.1029/1998JD200047, 1998.

Dong, X., Mace, G. G., Minnis, P., Smith, W. L., Poellot, M., Marchand, R. T., and Rapp, A. D.: Comparison of Stratus Cloud Properties Deduced from Surface, GOES, and Aircraft Data during the March 2000 ARM Cloud IOP, J. Atmos. Sci., 59, 3265–3284, https://doi.org/10.1175/1520-0469(2002)059<3265:coscpd>2.0.co;2, 2002.

Dong, X., & Mace, G. G.: Profiles of Low-Level Stratus Cloud Microphysics Deduced from Ground-Based Measurements, Journal of Atmospheric & Oceanic Technology, 20(1), 42-53, https://doi.org/10.1175/1520-0426(2003)020<0042:POLLSC>2.0.CO;2, 2003.

Dong, X., Xi, B., Kennedy, A., Minnis, P., & Wood, R.: A 19-Month Record of Marine Aerosol–Cloud–Radiation Properties Derived from DOE ARM Mobile Facility Deployment at the Azores. Part I: Cloud Fraction and Single-Layered MBL Cloud Properties, J. Climate, 27, 3665–3682, https://doi.org/10.1175/JCLI-D-13-00553.1, 2014.

Dong, X., Das, A., Xi, B., Zheng, X., Behrangi, A., Marcovecchio, A. R., & Girone, D. J.: Quantifying the differences in Southern Ocean clouds observed by radar and lidar from three platforms. Geophysical Research Letters, 52, e2024GL112079. https://doi.org/10.1029/2024GL112079, 2025

Doviak, R. J., & Zrnić, D. S.: Precipitation Measurements, in: *Doppler Radar and Weather Observations*, 2nd Edn., edited by: Doviak, R. J., and Zrnić, D. S., Academic Press, San Diego, CA, 209–279, https://doi.org/10.1016/B978-0-12-221422-6.50013-9, 1993.

Eloranta, E. E.: High Spectral Resolution Lidar, In C. Weitkamp (Ed.), Lidar: Range-Resolved Optical Remote Sensing of the Atmosphere (pp. 143–163), Springer, https://doi.org/10.1007/0-387-25101-4_5, 2005.

Esselborn, M., Wirth, M., Fix, A., Tesche, M., & Ehret, G.: Airborne high spectral resolution lidar for measuring aerosol extinction and backscatter coefficients, Applied Optics, 47(3), 346–358, https://doi.org/10.1364/AO.47.000346, 2008.

Ewald, F., Groß, S., Wirth, M., Delanoë, J., Fox, S., & Mayer, B.: Why we need radar, lidar, and solar radiance observations to constrain ice cloud microphysics, Atmospheric Measurement Techniques, 14(7), 5029–5047, https://doi.org/10.5194/amt-14-5029-2021, 2021.

Faber, S., French, J. R., and Jackson, R.: Laboratory and in-flight evaluation of measurement uncertainties from a commercial Cloud Droplet Probe (CDP), Atmos. Meas. Tech., 11, 3645–3659, https://doi.org/10.5194/amt-11-3645-2018, 2018.

Hogan, R. J., Gaussiat, N., and Illingworth, A. J.: Stratocumulus Liquid Water Content from Dual-Wavelength Radar, J. Atmos. Oceanic Technol., 22, 1207–1218, https://doi.org/10.1175/JTECH1768.1, 2005.

https://doi.org/10.5194/egusphere-2025-874
Preprint. Discussion started: 2 June 2025

Hu, Y., Rodier, S., Xu, K., Sun, W., Huang, J., Lin, B., Zhai, P., & Josset, D.: Occurrence, liquid water content, and fraction of supercooled water clouds from combined CALIOP/IIR/MODIS measurements, Journal of Geophysical Research: Atmospheres, 115(D4), https://doi.org/10.1029/2010JD014002, 2010.

Huang, D., Johnson, K., Liu, Y., and Wiscombe, W.: High resolution retrieval of liquid water vertical distributions using collocated Ka-band and W-band cloud radars, Geophys. Res. Lett., 36, L24807, https://doi.org/10.1029/2009GL041364, 2009.

Intrieri, J. M., Shupe, M. D., Uttal, T., & McCarty, B. J.: An annual cycle of Arctic cloud characteristics observed by radar and lidar at SHEBA, Journal of Geophysical Research: Oceans, 107(C10), SHE-5, https://doi.org/10.1029/2000JC000423, 2002.

Jackson, R. C., McFarquhar, G. M., Korolev, A. V., Earle, M. E., Liu, P. S. K., Lawson, R. P., Brooks, S., Wolde, M., Laskin, A., and Freer, M.: The dependence of ice microphysics on aerosol concentration in arctic mixed-phase stratus clouds during ISDAC and M-PACE: AEROSOL EFFECTS ON ARCTIC STRATUS, J. Geophys. Res. Atmospheres, 117, n/a-n/a, https://doi.org/10.1029/2012JD017668, 2012.

Kang, L., Marchand, R., & Smith, W.: Evaluation of MODIS and Himawari-8 low clouds retrievals over the Southern Ocean with in situ measurements from the SOCRATES campaign, Earth and Space Science, 8(3), e2020EA001397, https://doi.org/10.1029/2020EA001397, 2021.

Kang, L., Marchand, R. T., & Wood, R.: Stratocumulus precipitation properties over the Southern Ocean observed from aircraft during the SOCRATES campaign, Journal of Geophysical Research: Atmospheres, 129(6), e2023JD039831, https://doi.org/10.1029/2023JD039831, 2024.

Kay, J. E., Wall, C., Yettella, V., Medeiros, B., Hannay, C., Caldwell, P., & Bitz, C.: Global climate impacts of fixing the Southern Ocean shortwave radiation bias in the Community Earth System Model (CESM), Journal of Climate, 29(12), 4617–4636, https://doi.org/10.1175/JCLI-D-15-0358.1, 2016.

Klein, S. A., Hall, A., Norris, J. R., & Pincus, R.: Low-cloud feedbacks from cloud-controlling factors: A review, Shallow clouds, water vapor, circulation, and climate sensitivity, Springer, 135–157, 2018.

Kollias, P., Albrecht, B. A., and Marks, F.: Why Mie?, Bull. Amer. Meteor. Soc., 83, 1471–1484, https://doi.org/10.1175/BAMS-83-10-1471, 2002.

Korolev, A., & Milbrandt, J.: How are mixed-phase clouds mixed?, Geophysical Research Letters, 49(18), e2022GL099578, https://doi.org/10.1029/2022GL099578, 2022.

Lance, S., et al.: Water droplet calibration of the Cloud Droplet Probe (CDP) and in-flight performance in liquid, ice and mixed-phase clouds during ARCPAC, Atmos. Meas. Tech., 3, 1683-1706, https://doi.org/10.5194/amt-3-1683-2010, 2010.

Lawson, R. P., O'Connor, D., Zmarzly, P., Weaver, K., Baker, B., Mo, Q., & Jonsson, H.: The 2D-S (stereo) probe: Design and preliminary tests of a new airborne, high-speed, high-resolution particle imaging probe, Journal of Atmospheric and Oceanic Technology, 23(11), 1462–1477, https://doi.org/10.1175/JTECH1929.1, 2006.

Lawson, R. P., Pilson, B., Baker, B., Mo, Q., Jensen, E., Pfister, L., & Bui, P.: Aircraft measurements of microphysical properties of subvisible cirrus in the tropical tropopause layer, Atmospheric Chemistry and Physics, 8(6), 1609–1620, https://doi.org/10.5194/acp-8-1609-2008, 2008.

Liljegren, J. C., E. E. Clothiaux, G. G. Mace, S. Kato, and X. Dong: A new retrieval for cloud liquid water path using a ground-based microwave radiometer and measurements of cloud temperature. J. Geophys. Res., 106, 14 485–14 500, doi:10.1029/2000JD900817, 2001.

Mace, G. G., Protat, A., Humphries, R. S., Alexander, S. P., McRobert, I. M., Ward, J., Selleck, P., Keywood, M., & McFarquhar, G. M.: Southern Ocean cloud properties derived from CAPRICORN and MARCUS data, Journal of Geophysical Research: Atmospheres, 126(4), e2020JD033368, https://doi.org/10.1029/2020JD033368, 2021.

Maciel, F. V., Diao, M., and Yang, C. A.: Partition between supercooled liquid droplets and ice crystals in mixed-phase clouds based on airborne in situ observations, Atmos. Meas. Tech., 17, 4843–4861, https://doi.org/10.5194/amt-17-4843-2024, 2024.

Marcovecchio, A. R., Xi, B., Zheng, X., Wu, P., Dong, X., & Behrangi, A.: What Are the Similarities and Differences in Marine Boundary Layer Cloud and Drizzle Microphysical Properties During the ACE-ENA and MARCUS Field Campaigns?, Journal of Geophysical Research: Atmospheres, 128(18), e2022JD037109, https://doi.org/10.1029/2022JD037109, 2023.

Matus, A. V. and L'Ecuyer, T. S.: The role of cloud phase in Earth's radiation budget, J. Geophys. Res. Atmospheres, 122, 2559–2578, https://doi.org/10.1002/2016JD025951, 2017.

McCoy, D. T., Hartmann, D. L., & Grosvenor, D. P.: Observed Southern Ocean cloud properties and shortwave reflection. Part II: Phase changes and low cloud feedback, Journal of Climate, 27(23), 8858–8868, https://doi.org/10.1175/JCLI-D-14-00288.1, 2014.

McFarquhar, G.: Measurements of Aerosols, Radiation, and Clouds over the Southern Oceans (MARCUS) Science Plan, United States, https://doi.org/10.2172/1253914, 2016.

McFarquhar, G. M., Finlon, J. A., Stechman, D. M., Wu, W., Jackson, R. M., & Freer, M.: University of Illinois/Oklahoma Optical Array Probe (OAP) Processing Software. Version 3.1.4, Zenodo [code], https://doi.org/10.5281/zenodo.1285969, 2018.

McFarquhar, G. M., Bretherton, C., Marchand, R. T., DeMott, P. J., Alexander, S. P., Protat, A., Roberts, G., Twohy, C. H., Toohey, D. W., Siems, S., et al.: New Unique Observations of Clouds, Aerosols and Precipitation over the Southern Ocean: An Overview of SOCRATES and MARCUS, in: Proceedings of the 15th Conference on Cloud Physics/15th Conference on Atmospheric Radiation, AMS, 2018.

McFarquhar, G. M., Bretherton, C. S., Marchand, R., Protat, A., DeMott, P. J., Alexander, S., Rintoul, S. R., Roberts, G. C., Twohy, C. H., Toohey, D. W., et al.: Airborne, ship- and ground-based observations of clouds, aerosols and precipitation from recent field projects over the Southern Ocean, in: Proceedings of the AGU Fall Meeting, Washington, D.C., USA, 10-14 December 2018, A53D-06, 2018.

McFarquhar, G., Maarchang, R., Bretherton, C., Alexander, S., Protat, A., Siems, S., et al.: Measurements of aerosols, radiation, and clouds over the Southern Ocean (MARCUS) field campaign report, DOE/SC-ARM-008, U.S. Department of Energy, https://www.osti.gov/servlets/purl/1524775, 2019.

McFarquhar, G. M., Bretherton, C. S., Marchand, R., Protat, A., DeMott, P. J., Alexander, S. P., Roberts, G. C., Twohy, C. H., Toohey, D., Siems, S., et al.: Observations of clouds, aerosols, precipitation, and surface radiation over the Southern Ocean: An overview of CAPRICORN, MARCUS, MICRE, and SOCRATES, Bulletin of the American Meteorological Society, 102(4), E894–E928, https://doi.org/10.1175/BAMS-D-20-0132.1, 2021.

McGill, M., Hlavka, D., Hart, W., Scott, V. S., Spinhirne, J., & Schmid, B.: Cloud physics lidar: Instrument description and initial measurement results, Applied Optics, 41(18), 3725–3734, https://doi.org/10.1364/AO.41.003725, 2002.

Mioche, G., Jourdan, O., Ceccaldi, M., and Delanoë, J.: Variability of mixed-phase clouds in the Arctic with a focus on the Svalbard region: a study based on spaceborne active

https://doi.org/10.5194/egusphere-2025-874
Preprint. Discussion started: 2 June 2025

remote sensing, Atmospheric Chem. Phys., 15, 2445–2461, https://doi.org/10.5194/acp-15-2445-2015, 2015.

Mioche, G., Jourdan, O., Delanoë, J., Gourbeyre, C., Febvre, G., Dupuy, R., Monier, M., Szczap, F., Schwarzenboeck, A., and Gayet, J.-F.: Vertical distribution of microphysical properties of Arctic springtime low-level mixed-phase clouds over the Greenland and Norwegian seas, Atmos. Chem. Phys., 17, 12845–12869, https://doi.org/10.5194/acp-17-12845-2017, 2017.

Mohrmann, J., Finlon, J., Atlas, R., Lu, J., Hsiao, I., and Wood, R.: University of Washington Ice-Liquid Discriminator single particle phase classifications and 1 Hz particle size distributions/heterogeneity estimate, version 1.0, UCAR/NCAR - Earth Observing Laboratory [data set], https://doi.org/10.26023/PA5W-4DRX-W50A, 2021.

Moser, M., Voigt, C., Jurkat-Witschas, T., Hahn, V., Mioche, G., Jourdan, O., Dupuy, R., Gourbeyre, C., Schwarzenboeck, A., Lucke, J., Boose, Y., Mech, M., Borrmann, S., Ehrlich, A., Herber, A., Lüpkes, C., and Wendisch, M.: Microphysical and thermodynamic phase analyses of Arctic low-level clouds measured above the sea ice and the open ocean in spring and summer, Atmospheric Chem. Phys., 23, 7257–7280, https://doi.org/10.5194/acp-23-7257-2023, 2023.

NCAR/EOL HSRL Team: Gulfstream V High Spectral Resolution Lidar (GV-HSRL), UCAR/NCAR - Earth Observing Laboratory [data set], https://doi.org/10.5065/d67w6976, 2012.

NCAR/EOL HCR Team: HIAPER Cloud Radar (HCR), UCAR/NCAR - Earth Observing Laboratory [data set], https://doi.org/10.5065/D6BP00TP, 2014.

NCAR/EOL HCR Team, NCAR/EOL HSRL Team: SOCRATES: NCAR HCR radar and HSRL lidar moments data. Version 3.2, UCAR/NCAR - Earth Observing Laboratory [data set], https://doi.org/10.5065/D64J0CZS, 2023.

Oh, S.-B., Lee, Y. H., Jeong, J.-H., Kim, Y.-H., and Joo, S.: Estimation of the liquid water content and Z–LWC relationship using Ka-band cloud radar and a microwave radiometer, Meteorological Applications, 25, 423–434, https://doi.org/10.1002/met.1710, 2018.

Qiu, S., Dong, X., Xi, B., and Li, J.-L.F.: Characterizing Arctic mixed-phase cloud structure and its relationship with humidity and temperature inversion using ARM NSA observations, Journal of Geophysical Research: Atmospheres, 120, 7737–7746, https://doi.org/10.1002/2014JD023022, 2015.

Romatschke, U., Dixon, M., Tsai, P., Loew, E., Vivekanandan, J., Emmett, J., and Rilling, R.: The NCAR Airborne 94-GHz Cloud Radar: Calibration and Data Processing, Data, 6, 66, https://doi.org/10.3390/data6060066, 2021.

Romatschke, U., and Vivekanandan, J.: Cloud and precipitation particle identification using cloud radar and lidar measurements: Retrieval technique and validation, Earth and Space Science, 9, e2022EA002299, https://doi.org/10.1029/2022EA002299, 2022.

Sassen, K.: The Polarization Lidar Technique for Cloud Research: A Review and Current Assessment, Bulletin of the American Meteorological Society, 72, 1848–1866, http://www.jstor.org/stable/26228894, 1991.

Schima, J., McFarquhar, G., Romatschke, U., Vivekanandan, J., D'Alessandro, J., Haggerty, J., et al.: Characterization of Southern Ocean Boundary Layer Clouds using airborne radar, lidar, and in situ cloud data: Results from SOCRATES, Journal of Geophysical Research: Atmospheres, 127, e2022JD037277, https://doi.org/10.1029/2022JD037277, 2022.

Shupe, M. D., Kollias, P., Matrosov, S. Y., and Schneider, T. L.: Deriving mixed-phase cloud properties from Doppler radar spectra, J. Atmos. Oceanic Technol., 21, 660–670, https://doi.org/10.1175/1520-0426(2004)021<0660>2.0.CO;2, 2004.

https://doi.org/10.5194/egusphere-2025-874
Preprint. Discussion started: 2 June 2025

Shupe, M. D., Uttal, T., and Matrosov, S. Y.: Arctic Cloud Microphysics Retrievals from Surface-Based Remote Sensors at SHEBA, Journal of Applied Meteorology and Climatology, 44, 1544–1562, https://doi.org/10.1175/JAM2297.1, 2005.

Shupe, M. D.: A ground-based multisensor cloud phase classifier, Geophysical Research Letters, 34, L22809, https://doi.org/10.1029/2007GL031008, 2007.

Song, J. I., Yum, S. S., Park, S.-H., Kim, K.-H., Park, K.-J., & Joo, S.-W.: Climatology of melting layer heights estimated from cloud radar observations at various locations. Journal of Geophysical Research: Atmospheres, 126, e2021JD034816. https://doi.org/10.1029/2021JD034816, 2021

Su, W., Schuster, G. L., Loeb, N. G., Rogers, R. R., Ferrare, R. A., Hostetler, C. A., Hair, J. W., and Obland, M. D.: Aerosol and cloud interaction observed from high spectral resolution lidar data, J. Geophys. Res., 113, D24202, https://doi.org/10.1029/2008JD010588, 2008.

Trenberth, K. E., and Fasullo, J. T.: Simulation of present-day and twenty-first-century energy budgets of the Southern Oceans, Journal of Climate, 23, 440–454, https://doi.org/10.1175/2009JCLI3152.1, 2010.

UCAR/NCAR - Earth Observing Laboratory: NSF/NCAR GV HIAPER Raw 2D-S Imagery, Version 1.1, UCAR/NCAR - Earth Observing Laboratory [data set], https://doi.org/10.26023/9555-DKY0-J604, 2018.

UCAR/NCAR - Earth Observing Laboratory. SOCRATES: Low Rate (LRT - 1 sps) Navigation, State Parameter, and Microphysics Flight-Level Data, Version 1.4, UCAR/NCAR - Earth Observing Laboratory [data set], https://doi.org/10.5065/D6M32TM9, 2022.

Vivekanandan, J., Ellis, S., Tsai, P., Loew, E., Lee, W.-C., Emmett, J., et al.: A wing pod-based millimeter wavelength airborne cloud radar, Geoscientific Instrumentation, Methods and Data Systems, 4, 161–176, https://doi.org/10.5194/gi-4-161-2015, 2015.

Vivekanandan, J., Ghate, V. P., Jensen, J. B., Ellis, S. M., and Schwartz, M. C.: A Technique for Estimating Liquid Droplet Diameter and Liquid Water Content in Stratocumulus Clouds Using Radar and Lidar Measurements, Journal of Atmospheric and Oceanic Technology, 37, 2145–2161, https://doi.org/10.1175/JTECH-D-19-0092.1, 2020.

Wang, Y., Zhang, D., Liu, X., and Wang, Z.: Distinct contributions of ice nucleation, large-scale environment, and shallow cumulus detrainment to cloud phase partitioning with NCAR CAM5, Journal of Geophysical Research: Atmospheres, 123, 1132–1154, https://doi.org/10.1002/2017JD027213, 2018.

Wang, Z., and Sassen, K.: Cloud Type and Macrophysical Property Retrieval Using Multiple Remote Sensors, Journal of Applied Meteorology, 40, 1665–1682, https://doi.org/10.1175/1520-0450(2001)040<1665>2.0.CO;2, 2001.

Wang, Z., Wechsler, P., Kuestner, W., French, J., Rodi, A., Glover, B., Burkhart, M., and Lukens, D.: Wyoming Cloud Lidar: instrument description and applications, Optics Express, 17, 13576–13587, https://doi.org/10.1364/OE.17.013576, 2009.

Wang, Z., French, J., Vali, G., Wechsler, P., Haimov, S., Rodi, A., Deng, M., Leon, D., Snider, J., Peng, L., and Pazmany, A. L.: Single Aircraft Integration of Remote Sensing and In Situ Sampling for the Study of Cloud Microphysics and Dynamics, Bulletin of the American Meteorological Society, 93, 653–668, https://doi.org/10.1175/BAMS-D-11-00044.1, 2012.

Wood, R.: Drizzle in stratiform boundary layer clouds. Part I: Vertical and horizontal structure, J. Atmos. Sci., 62, 3011–3033, https://doi.org/10.1175/JAS3529.1, 2005.

Wu, P., Dong, X., Xi, B., Tian, J., and Ward, D. M.: Profiles of MBL cloud and drizzle microphysical properties retrieved from ground-based observations and validated by

https://doi.org/10.5194/egusphere-2025-874
Preprint. Discussion started: 2 June 2025

aircraft in situ measurements over the Azores, Journal of Geophysical Research: Atmospheres, 125, e2019JD032205, https://doi.org/10.1029/2019JD032205, 2020a.

Wu, P., Dong, X., and Xi, B.: A Climatology of Marine Boundary Layer Cloud and Drizzle Properties Derived from Ground-Based Observations over the Azores, Journal of Climate, 33, 10133–10148, https://doi.org/10.1175/JCLI-D-20-0272.1, 2020b.

Wu, W., and McFarquhar, G. M.: On the Impacts of Different Definitions of Maximum Dimension for Nonspherical Particles Recorded by 2D Imaging Probes, Journal of Atmospheric and Oceanic Technology, 33, 1057–1072, https://doi.org/10.1175/JTECH-D-15-0177.1, 2016.

Wu, W., and McFarquhar, G.: NSF/NCAR GV HIAPER 2D-S Particle Size Distribution (PSD) Product Data. Version 1.1, UCAR/NCAR - Earth Observing Laboratory [data set], https://doi.org/10.26023/8HMG-WQP3-XA0X, 2019.

Xi, B., Dong, X., Minnis, P., and Khaiyer, M. M.: A 10 year climatology of cloud fraction and vertical distribution derived from both surface and GOES observations over the DOE ARM SPG site, Journal of Geophysical Research, 115, D12124, https://doi.org/10.1029/2009JD012800, 2010.

Xi, B., Dong, X., Zheng, X., and Wu, P.: Cloud phase and macrophysical properties over the Southern Ocean during the MARCUS field campaign, Atmospheric Measurement Techniques, 15, 3761–3777, https://doi.org/10.5194/amt-15-3761-2022, 2022.

Zaremba, T. J., Rauber, R. M., McFarquhar, G. M., Hayman, M., Finlon, J. A., and Stechman, D. M.: Phase characterization of cold sector Southern Ocean Cloud tops: Results from SOCRATES, Journal of Geophysical Research: Atmospheres, 125, e2020JD033673, https://doi.org/10.1029/2020JD033673, 2020.

Zhao, L., Zhao, C., Wang, Y., Wang, Y., and Yang, Y.: Evaluation of cloud microphysical properties derived from MODIS and Himawari-8 using in situ aircraft measurements over the Southern Ocean, Earth and Space Science, 7, e2020EA001137, https://doi.org/10.1029/2020EA001137, 2020.

Zhao, X., Liu, X., Burrows, S., DeMott, P. J., Diao, M., McFarquhar, G. M., Patade, S., Phillips, V., Roberts, G. C., Sanchez, K. J., et al.: Important ice processes are missed by the Community Earth system model in Southern Ocean mixed-phase clouds: Bridging SOCRATES observations to model developments, Journal of Geophysical Research: Atmospheres, 128, e2022JD037513, https://doi.org/10.1029/2022JD037513, 2023.

Zheng, X., Xi, B., Dong, X., Logan, T., Wang, Y., and Wu, P.: Investigation of aerosol–cloud interactions under different absorptive aerosol regimes using Atmospheric Radiation Measurement (ARM) southern Great Plains (SGP) ground-based measurements, Atmos. Chem. Phys., 20, 3483–3501, https://doi.org/10.5194/acp-20-3483-2020, 2020.

Zheng, X., Dong, X., Xi, B., Logan, T., and Wang, Y.: Distinctive aerosol–cloud–precipitation interactions in marine boundary layer clouds from the ACE-ENA and SOCRATES aircraft field campaigns, Atmos. Chem. Phys., 24, 10323–10347, https://doi.org/10.5194/acp-24-10323-2024, 2024.